

**Nonlinear optics at low powers:
new mechanism of on-chip optical frequency comb generation**

Andrei Rogov^{1,*} and Evgenii Narimanov¹

¹*Birck Nanotechnology Center, School of Electrical and Computer Engineering,
Purdue University, West Lafayette, Indiana 47907, USA*

Nonlinear optical effects provide a natural way of light manipulation and interaction, and form the foundation of applied photonics – from high-speed signal processing and telecommunication [1–5], to ultra-high bandwidth interconnects [6–9] and information processing [10–12]. However, relatively weak nonlinear response at optical frequencies [13] calls for operation at high optical powers, or boosting efficiency of nonlinear parametric processes by enhancing local field intensity with high quality-factor resonators near cavity resonance, resulting in reduced operational bandwidth and increased loss due to multi-photon absorption. Here, we present an alternative to this conventional approach, with strong nonlinear optical effects at substantially lower local intensities, based on period-doubling bifurcations near nonlinear cavity anti-resonance, and apply it to low-power optical frequency comb generation [14, 15] in a silicon chip.

* arogov@purdue.edu

I. INTRODUCTION

In the never-ending quest for higher signal processing speeds, optics-based systems represent an attractive research direction, since, in contrast to the well-studied area of electronics, optical domain is perfectly suitable for operation at high frequencies. The basis for any signal processing is manipulation of signals, or light waves, as in the case of optics. Medium nonlinearity provides a means of interaction of different propagating waves with each other and the medium itself.

Two strategies have been traditionally used to enhance nonlinear optical effects: (1) targeting materials with high optical nonlinearities, such as chalcogenide glasses [16, 17], silicon [2, 18], AlGaAs [19, 20], and (2) employing resonant structures to increase local field intensity. The choice of material is oftentimes dictated by fabrication limitations and the overall design compatibility requirements. For example, due to its lower cost and direct compatibility with the well developed CMOS industry, silicon-based nonlinear photonics has gained a lot of interest in the last decade [21]. On the other hand, resonators offer significant enhancement of local field intensity at the resonance regime, which allowed for experimental observation of nonlinear optical effects in fibre resonators at first [22–24], and then, with the development of microfabrication, in high quality-factor (Q) microresonators [9, 25–40]. However, boosting local field intensities with high- Q resonators for enhancing nonlinearity has its disadvantages. First, high intracavity intensities lead to significant multi-photon absorption losses, which makes this resonant approach inapplicable to the materials with substantial nonlinear losses, such as silicon at the telecom wavelength of 1550 nm [41]. Second, ultra-high- Q microresonators, which allow for observation of nonlinear effects at the lowest power, are extremely sensitive to fabrication non-idealities and suffer from poor scalability and on-chip integrability. Finally, high- Q microresonators at the resonance are highly susceptible to external perturbations – up to individual molecules – which is advantageous for nanoparticle detection systems [42–44], but detrimental to many other applications. As we show in this work, nonlinear effects in microresonators can also be observed in near-anti-resonance regime, which, in contrast to the standard resonant approach, naturally implies low intracavity intensity operation, and, as a consequence, is much less prone to the aforementioned disadvantages.

Effects of nonlinearity on a system dynamics can often be understood by introducing the concept of modulation instability. If a stable state of the system corresponds to a uniform carrier wave propagating in nonlinear dispersive medium, an unstable state can be viewed as a modulated carrier wave. Such a modulation instability (MI) caused by the interplay between nonlinear and dispersive effects has been observed in many areas of physics [45], including nonlinear optics, where

it manifests itself as breakup of continuous wave (CW) radiation into a train of ultra-short pulses [46]. When a CW beam propagates through a nonlinear dispersive optical medium, anomalous dispersion is required for the modulation instability to occur. However, in the presence of a feedback, as in the case of a resonator system, modulation instability can arise even at normal dispersion, and occurs either close to the cavity resonance, or close to a cavity anti-resonance [23]. Therefore, nonlinear effects in resonators should be expected both in the resonance and anti-resonance regime. Motivated by the advantages of low intracavity intensity operation, we are studying the effects of nonlinearity in a resonator system in the vicinity of the cavity anti-resonance, and applying this approach to low-power optical frequency comb generation in a silicon chip at the telecom wavelength.

II. NEW MECHANISM (SINGLE RESONATOR SYSTEM)

In the antiresonant regime, the nonlinear dynamics of the single resonator system is affected by period-doubling instabilities [23]: an increased effective nonlinearity in the resonator brakes the system integrability, which results in period-doubling transition to chaos [47]. If CW-states are considered stable period-1 states, period-doubling bifurcations lead to the formation of regions in the system parameter space with stable states of higher periods – stationary states with multiple wave amplitude values. Existence of higher-period stable states leads to switching in time-domain: the system traverses the set of allowed stable wave amplitude values in sequence switching between them within the system characteristic time period (round-trip time in the resonator). Periodic switching in time-domain translates to the comb spectrum in frequency domain.

If the linear (intensity-independent) part of the phase shift accumulated per round trip in the cavity places it near its resonance, significant non-linear (intensity-induced) phase shift ($\phi_{NL} \approx \pi$) is required to tune the cavity close to its anti-resonance, and period-doubling bifurcations are observed at impractically high optical powers [48].

On the other hand, if the linear phase shift per round trip puts the “cold cavity” (cavity at sufficiently low intensities, such that high-intensity effects can be neglected) close to its anti-resonance, little non-linear phase shift ($|\phi_{NL}| \ll \pi$) is required for the system to reach the higher-period stable state. As a result, period-doubling bifurcations, and frequency comb generation in particular, in principle, could be achieved at close to zero intracavity intensities. For real applications low intracavity power means negligibly low multi-photon absorption losses. This is the key idea behind the new mechanism we propose.

In order to clarify the main features of the suggested mechanism, we first consider a single resonator system without group velocity dispersion (GVD), with a microring resonator coupled to the waveguide (Fig. 1a) used both to pump the resonator and to direct the output signal.

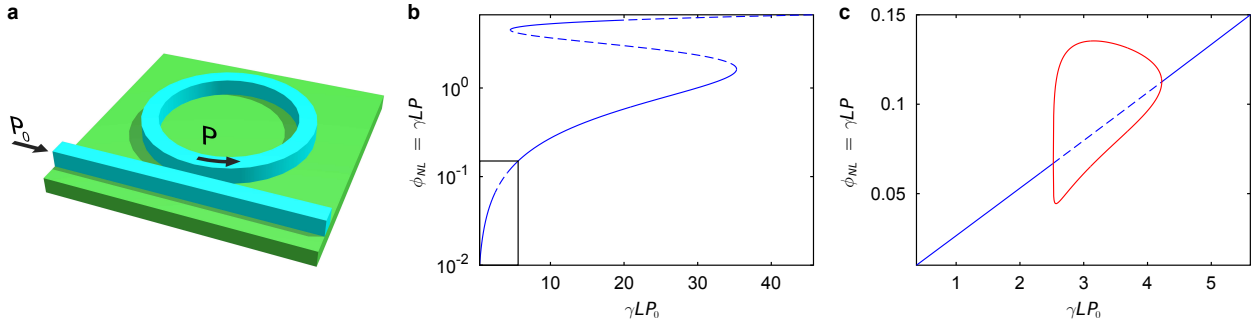


FIG. 1. (a) Schematics of the microring resonator system. (b) Period-1 stable (solid line) and unstable (dashed) states with highlighted first instability region (black rectangle contour) (c) Bifurcation diagram of the first period-1 instability region for the steady states of the power P inside the microring at different values of the power P_0 in the waveguide (excitation power). Shown in blue and red are fixed points of period-1 and period-2 respectively. Coloured solid lines represent stable fixed points, dashed – unstable. The simulation data were obtained for a resonator with ring radius $R = 10 \mu\text{m}$, $\kappa^2 = 0.1$, $\phi = \pi - 0.14$, $\alpha = 0.7 \text{ dB/cm}$, and TPA as in silicon near $\lambda = 1550 \text{ nm}$.

The wave propagation inside the microring can be described by the nonlinear Schrödinger's equation:

$$\frac{\partial A}{\partial z} = i\gamma(1+ir)|A|^2A - \frac{\alpha}{2}A = 0 \quad (1)$$

where A is the normalized wave packet amplitude ($|A|^2$ has the units of power), γ is the nonlinearity coefficient, r is the two-photon absorption (TPA) coefficient ($r \approx 0.1$ for silicon), α is the power attenuation constant, and $T \equiv t - z/v_g$ is time in the frame of reference moving with the wave packet at the group velocity v_g , while the coupling of the resonator to the waveguide can be modelled by the matrix equation:

$$\begin{bmatrix} b(t) \\ d(t) \end{bmatrix} = \begin{bmatrix} \tau & \kappa \\ -\kappa^* & \tau^* \end{bmatrix} \begin{bmatrix} a(t) \\ c(t) \end{bmatrix} \quad (2)$$

where τ and κ are respectively the amplitude transmission and coupling coefficients for the coupler between the microring and the waveguide, $a \equiv A(z = L)$ (L is the circumference of the resonator) and $b \equiv A(z = 0)$, while the amplitudes c and d correspond to the field amplitudes at the “input” and “through” ports of the waveguide. The system dynamics governed by Eqs. (1) and (2) can be

described by the nonlinear map:

$$b^{(n+1)} = \tau a^{(n+1)} + \kappa c \quad (3)$$

$$a^{(n+1)} = \frac{\exp\left(-\frac{\alpha}{2}L\right)}{\sqrt{1+2r\gamma\tilde{L}|b^{(n)}|^2}} \exp\left[\frac{i\log\left(1+2r\gamma\tilde{L}|b^{(n)}|^2\right)}{2r}\right] \exp(i\phi)b^{(n)} \quad (4)$$

where

$$\tilde{L} = \frac{1 - \exp(-\alpha L)}{\alpha} \quad (5)$$

and it was assumed that $c(t) \equiv c = \text{const}$ as in the case of pumping the resonator with a CW light source, ϕ is the intensity- and frequency-independent constant phase shift per one round-trip in the microring.

Stability analysis of the map (3)-(4) shows that the system has multiple regions of period-1 stable and unstable states (Fig.1b). However, it is the very first region that allows for period-1 unstable states to exist at the lowest both intracavity P and excitation P_0 power, which is achieved when the resonator is tuned into the vicinity of anti-resonance. At the point where period-1 state loses stability, the system undergoes a period-doubling bifurcation which leads to the formation of period-2 stable state. This dynamics is illustrated in Fig.1c that depicts the lowest power period-2 bubble. The originally stable period-1 mode corresponding to the time-independent power inside the ring (solid blue curve in Fig.1c), eventually loses stability with increasing power and the system switches to a new period-2 stable mode – a state with the period $2T_c$ ($T_c = L/v_g$ – round-trip time) corresponding to two ring round-trips (solid red curve in Fig.1c). At this point, the steady-state power in the microring is no longer time-independent and the switching between the two power levels occurs (inset in Fig.1c), leading to multiple subbands in the power spectrum and frequency comb generation (Fig.2).

With a finite GVD present in the system, the instantaneous switching demonstrated earlier is replaced with smooth transitions (Fig.2b). Dispersion acting together with Kerr nonlinearity effectively limits the frequency comb spectrum: the stronger the GVD is, the less frequency components are visible (Fig.2c).

It should be emphasized that the proposed mechanism of frequency comb formation is qualitatively different from the well known approach [25, 29, 36]. According to the standard picture, all comb sidebands are formed at multiple or single free spectral ranges (FSR) away from the pump [29]. In contrast, in the suggested mechanism, the first harmonic is generated at $f_1 = \frac{FSR}{2} = \frac{1}{2T_c}$ away from the pump frequency, although the higher harmonics follow single FSR spacing (Fig.2c).

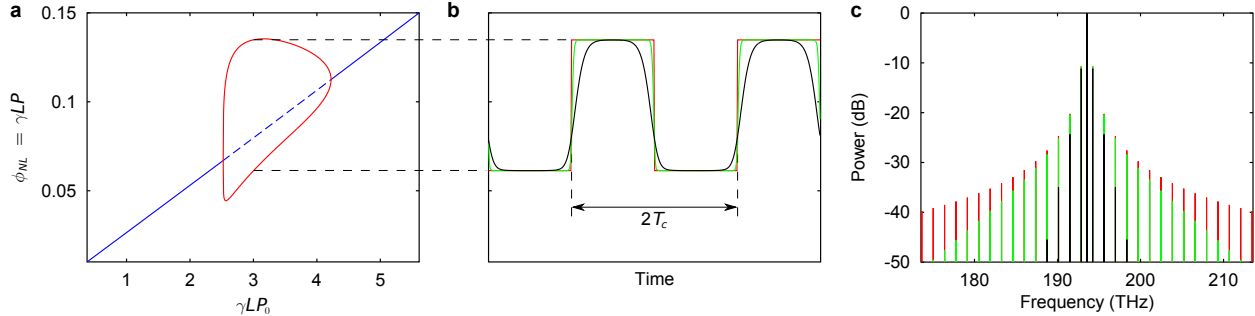


FIG. 2. Bifurcation diagram of the first period-1 instability region (a) and corresponding waveforms (b) and power spectra (c) inside a microring resonator. The red curve in (b) and (c) represents the case of zero GVD, with linear losses $\alpha = 0.7$ dB/cm throughout the frequency spectrum; green and black curves correspond to weak and strong normal GVD ($\beta_2 > 0$) respectively, with bulk material losses as in silicon and $\alpha = 0.7$ dB/cm at $\lambda = 1550$ nm ($f \approx 194$ THz). The simulation data were obtained for a resonator excited at $\lambda = 1550$ nm with the scaled excitation power $\gamma L P_0 = 3$, $\kappa^2 = 0.1$, $\phi = \pi - 0.14$, TPA as in silicon near $\lambda = 1550$ nm, and ring radius $R = 10 \mu\text{m}$.

Note that the bifurcation from period-1 to period-2 stable states (threshold point for frequency comb generation) takes place at the nonlinear phase shift per round trip $\phi_{NL}^{Th} \equiv \gamma L P^{Th} \approx 0.06 \ll 1$ (Fig.1c). Moreover, our analysis shows that the threshold intracavity power can be further decreased: $\phi_{NL}^{Th} \equiv \gamma L P^{Th} \sim \kappa^2$, with the optimally tuned linear phase $\phi \sim \pi - \kappa^2$, and the intracavity linear losses negligibly small compared to the nonlinear ones (valid approximation for the system with parameters given in Fig.1). Since the TPA-related loss is proportional to the intracavity power, and other multi-photon absorption processes exhibit even stronger power dependence, nonlinear losses are negligible, and linear losses become the limiting factor for the threshold intracavity power.

However, even though the intracavity power threshold can be low, the minimum excitation power threshold P_0^{Th} is quite high ($\gamma L P_0^{Th} \approx 2.5$), since the resonator is in anti-resonance regime. Low intracavity power leads to a possibility of using materials with high nonlinear losses, such as silicon at the telecom wavelength, while high excitation power prohibits the single resonator design discussed above from the practical implementation on a chip. In the next section we resolve this issue.

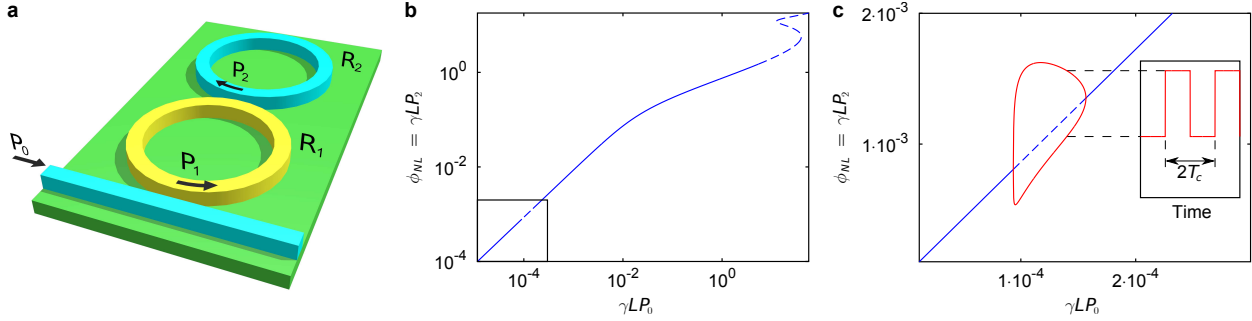


FIG. 3. (a) Schematics of the double resonator system: R_1 – linear microring resonator, R_2 – nonlinear. (b) Period-1 stable and unstable states with highlighted first instability region (black rectangle contour). (c) Bifurcation diagram of the first period-1 instability region for the steady states of the power P_2 inside R_2 at different values of the excitation power P_0 in the waveguide. Shown in blue and red are fixed points of period-1 and period-2 respectively. Coloured solid lines represent stable fixed points, dashed – unstable. Inset: waveforms inside R_2 at the scaled excitation power $\gamma LP_0 = 1.4 \cdot 10^{-4}$ at zero GVD. The simulation data were obtained for resonators with ring radii $R = 10 \mu\text{m}$, $\kappa_1^2 = 0.01$, $\kappa_2^2 = 0.1$, $\phi_1 = 0$, $\phi_2 = \pi - 1.7 \cdot 10^{-3}$, $\alpha = 0.7 \text{ dB/cm}$, and TPA in R_2 as in silicon near $\lambda = 1550 \text{ nm}$.

III. DOUBLE RESONATOR SYSTEM: A SOLUTION TO THE HIGH THRESHOLD EXCITATION POWER PROBLEM

As pointed out earlier, high threshold excitation power ($\gamma LP_0^{Th} \approx 2.5$) of the single resonator system prevents it from being effectively implemented on-chip. This issue can be resolved by introducing another resonator into the system (resonator R_1 in Fig.3a) operating at or near resonance [35, 39] and acting as a “pre-amplifier” between the input waveguide and the nonlinear resonator R_2 . To demonstrate the properties of the double resonator system, we first consider the extra resonator R_1 to be made of a linear optical material, with the case of both resonators made of the same nonlinear medium described in the following section.

Similarly to the single resonator system, we obtain the nonlinear map:

$$b_2^{(n+1)} = \tau_2 a_2^{(n+1)} + \tau_1 \kappa_2 a_1^{(n+1)} + \kappa_1 \kappa_2 c \quad (6)$$

$$a_2^{(n+1)} = \frac{\exp\left(-\frac{\alpha}{2}L\right)}{\sqrt{1 + 2r\gamma\tilde{L}|b_2^{(n)}|^2}} \exp\left[\frac{i \log\left(1 + 2r\gamma\tilde{L}|b_2^{(n)}|^2\right)}{2r}\right] \exp(i\phi_2) b_2^{(n)} \quad (7)$$

$$a_1^{(n+1)} = \exp\left(-\frac{\alpha}{2}L\right) \exp(i\phi_1) d_2^{(n)} \quad (8)$$

$$d_2^{(n)} = \frac{\tau_2^* b_2^{(n)} - a_2^{(n)}}{\kappa_2} \quad (9)$$

where we assumed the equal round-trip time $T_c = L/v_g$ in both resonators of equal circumference L for simplicity of the analysis, $c(t) \equiv c = \text{const}$ for CW-pumping, \tilde{L} is defined by Eq. (5) as before, ϕ_1 and ϕ_2 are the intensity- and frequency-independent constant phase shifts per one round-trip in resonators R_1 and R_2 correspondingly, τ_1 (κ_1) and τ_2 (κ_2) are the amplitude transmission (coupling) coefficients for the coupler between the waveguide and R_1 and between R_1 and R_2 respectively, γ and r are the nonlinearity and the TPA coefficients correspondingly of the nonlinear resonator R_2 .

As before, the stability analysis reveals multiple regions of period-1 stable and unstable states (Fig.3b) and confirms that the system has a bifurcation from period-1 to period-2 stable state when the resonator R_2 is tuned into the vicinity of anti-resonance (Fig.3c), as in the case of the single resonator, whereas the resonator R_1 is tuned into the near-resonance and provides the required power upconversion between the waveguide and the resonator R_2 . More than that, the stability analysis also shows that the double resonator system is more unstable than the considered earlier single resonator system, which is beneficial for frequency comb generation. Specifically, adding an extra resonator widens the instability regions and lowers the threshold excitation power as well as the intracavity powers: $\phi_{NL}^{Th} \equiv \gamma LP_2^{Th} \sim \kappa_1^2 \kappa_2^2$ (against $\phi_{NL}^{Th} \equiv \gamma LP^{Th} \sim \kappa^2$ in the single resonator system), with the optimally tuned linear phase $\phi_2 \sim \pi - \kappa_1^2 \kappa_2^2$, resonator R_1 in near-resonance regime, and negligible linear loss approximation as before; $\gamma LP_1^{Th} \sim \kappa_2^{-2} \gamma LP_2^{Th} \sim \kappa_1^2$ and $\gamma LP_0^{Th} \sim \kappa_1^2 \gamma LP_1^{Th} \sim \kappa_1^4$ (against $\gamma LP_0^{Th} = \text{const} \approx 2.5$ in the single resonator system). Therefore, in contrast to the case of the single resonator, the coupling between resonator R_1 and the waveguide in the suggested double resonator system can be designed so that the threshold excitation power is orders of magnitude lower ($\gamma LP_0^{Th} \approx 1 \cdot 10^{-4}$ in Fig.3c), which solves the high threshold excitation power problem.

However, even though such double resonator design could provide frequency comb generation at low excitation and intracavity powers theoretically, from a practical point of view it would be difficult to fabricate and couple two resonators made from different materials (R_1 – from a highly linear material, such as silica; R_2 – from a nonlinear material, such as silicon) on the same substrate. In the next section we show that the double resonator system still supports frequency comb generation at low powers even when both resonators are made from the same nonlinear material.

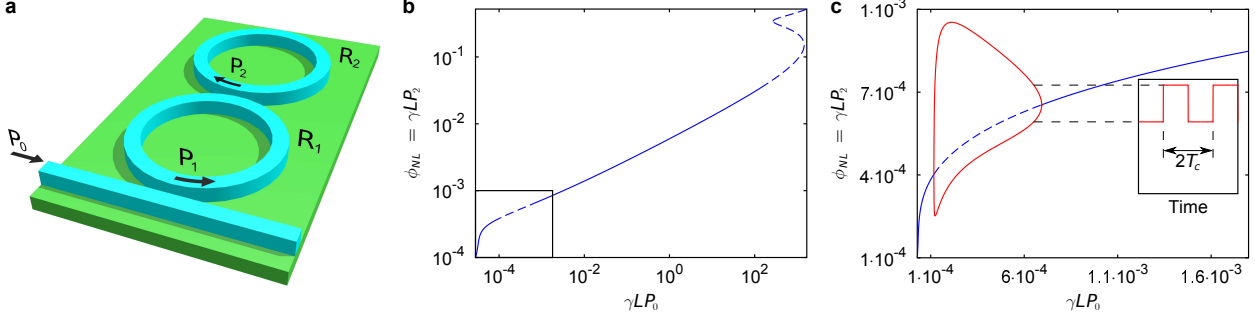


FIG. 4. (a) Schematics of the nonlinear double resonator system: R_1 and R_2 – nonlinear microring resonators. (b) Period-1 stable and unstable states with highlighted first instability region (black rectangle contour). (c) Bifurcation diagram of the first period-1 instability region for the steady states of the power P_2 inside R_2 at different values of the scaled excitation power P_0 in the waveguide. Shown in blue and red are fixed points of period-1 and period-2 respectively. Coloured solid lines represent stable fixed points, dashed – unstable. Inset: waveforms inside R_2 at the scaled excitation power $\gamma L P_0 = 6.5 \cdot 10^{-4}$ at zero GVD. The simulation data were obtained for resonators with ring radii $R = 10 \mu\text{m}$, $\kappa_1^2 = 0.01$, $\kappa_2^2 = 0.1$, $\phi_1 = -1 \cdot 10^{-2}$, $\phi_2 = \pi - 1.4 \cdot 10^{-3}$, $\alpha = 0.7 \text{ dB/cm}$, and TPA as in silicon near $\lambda = 1550 \text{ nm}$.

IV. NONLINEAR DOUBLE RESONATOR SYSTEM

Fabricating both resonators from the same nonlinear material would be easier for manufacturing reasons than making them from two different media, and, as in the case of silicon, would also be compatible with the standard silicon-based fabrication process. Since the double resonator system with a linear resonator R_1 is capable of frequency comb generation at low excitation as well as low intracavity powers, R_1 could be replaced with a nonlinear resonator equivalent to R_2 . Here we demonstrate that.

For the nonlinear double resonator system (Fig.4a) we obtain the nonlinear map:

$$b_2^{(n+1)} = \tau_2 a_2^{(n+1)} + \tau_1 \kappa_2 a_1^{(n+1)} + \kappa_1 \kappa_2 c \quad (10)$$

$$a_2^{(n+1)} = \frac{\exp\left(-\frac{\alpha}{2}L\right)}{\sqrt{1 + 2r\gamma\tilde{L}|b_2^{(n)}|^2}} \exp\left[\frac{i \log\left(1 + 2r\gamma\tilde{L}|b_2^{(n)}|^2\right)}{2r}\right] \exp(i\phi_2) b_2^{(n)} \quad (11)$$

$$a_1^{(n+1)} = \frac{\exp\left(-\frac{\alpha}{2}L\right)}{\sqrt{1 + 2r\gamma\tilde{L}|d_2^{(n)}|^2}} \exp\left[\frac{i \log\left(1 + 2r\gamma\tilde{L}|d_2^{(n)}|^2\right)}{2r}\right] \exp(i\phi_1) d_2^{(n)} \quad (12)$$

$$d_2^{(n)} = \frac{\tau_2^* b_2^{(n)} - a_2^{(n)}}{\kappa_2} \quad (13)$$

where we assumed the two resonators to be identical, each with the round-trip time $T_c = L/v_g$, circumference L , nonlinearity γ and the TPA r coefficients; $c(t) \equiv c = \text{const}$ for CW-pumping, \tilde{L} is defined by Eq. (5), $\phi_{1(2)}$, $\tau_{1(2)}$, and $\kappa_{1(2)}$ are defined the same way as before.

As seen from Fig.4b,c, the frequency comb generation is possible when the resonator R_2 is tuned into the vicinity of anti-resonance and the resonator R_1 is tuned into the near-resonance, just as in the previously considered case of the linear “pre-amplifier”. The intracavity power in R_1 is sufficiently low ($\gamma LP_1^{Th} \sim 10^{-2}$), so that the multi-photon absorption processes are negligible. Note that the value of the linear phase shift in R_1 is picked in such a way ($\phi_1 = -1 \cdot 10^{-2}$), that the resonator operates close to its resonance, but does not enter the bistability regime. As it could have been expected, with introducing nonlinearity in the resonator R_1 , the overall system becomes more unstable, which can be observed as broadening of the period-1 instability region – which makes the frequency comb generation regime accessible at wider range of excitation powers ($\gamma LP_0 \approx 1 \cdot 10^{-4} \dots 7 \cdot 10^{-4}$).

V. DISCUSSION

Now that we introduced a new (anti-resonant) mechanism of frequency comb generation, one of the key questions to answer is how it compares with the conventional (resonant) method [25, 29, 36]. First of all, as it was mentioned before, the anti-resonant mechanism has a specific spectral signature: the first harmonic is generated at $f_1^{(2)} = \frac{FSR}{2} = \frac{1}{2T_c}$ away from the pump frequency for a period-2 state ($f_1^{(n)} = \frac{FSR}{n} = \frac{1}{nT_c}$ for a period- n state), while in the resonant approach all harmonics are formed at multiple or single FSR away from the pump. Secondly, if the comb in the suggested mechanism arises as a consequence of the temporal pattern formation (intensity switching with each round-trip), comb generation in the conventional method is connected to the formation of spatial patterns, such as cavity solitons and Turing patterns, along the resonator circumference [49]. Thirdly, the group velocity dispersion is the key factor for pattern formation in the resonant approach, while the comb generation with the anti-resonant mechanism relies exclusively on the first-order dispersion (group velocity) for pattern formation and non-zero GVD only narrows the spectrum. The key role of GVD for pattern formation in the resonant case can be seen from the bifurcation diagram for zero-GVD case (Fig.1b): the system exhibits period-doubling instabilities near the cavity anti-resonances, which lead to the temporal pattern formation and frequency comb generation, while the system dynamics in the resonant regions is limited by bistable behaviour. Non-zero GVD enables interaction between adjacent infinitesimally short pulse slices propagating

along the resonator circumference and thus introducing a new (spatial) dimension into the nonlinear dynamics of the system, as well as spatial patterns and the resonant regime of frequency comb generation.

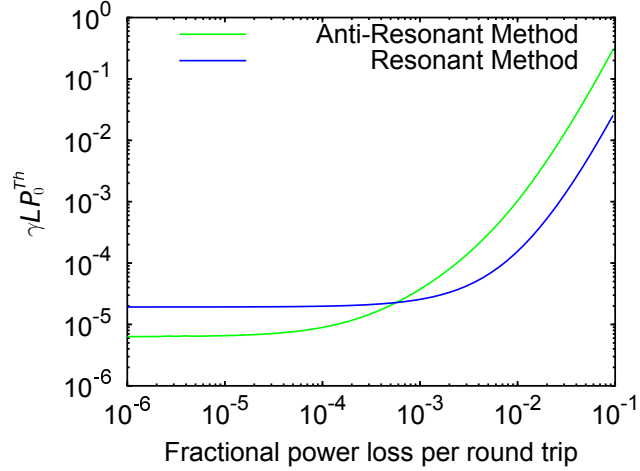


FIG. 5. Excitation power threshold for frequency comb generation in the resonant (blue curve) and anti-resonant (green curve) regimes at different levels of linear losses and without nonlinear losses. The simulation data were obtained in the resonant regime for the resonator with $\kappa^2 = 0.01$; in the anti-resonant regime – for the nonlinear double resonator system with $\kappa_1^2 = 0.01$, $\kappa_2^2 = 0.1$.

The threshold power for parametric oscillation in the resonant regime can be estimated as the threshold power for entering bistability regime in the zero-GVD case [33, 50]. In contrast, the threshold power for the anti-resonant frequency comb generation is determined by the first period-doubling bifurcation. Fig.5 illustrates the difference in threshold powers for frequency comb generation between the resonant and anti-resonant regimes. Thus, at low linear losses, the anti-resonant method demonstrates the lowest threshold power, while at high losses – resonant. However, note that Fig.5 shows the case of zero nonlinear losses: frequency comb generation in the resonant regime requires the resonator to be made from a material without nonlinear losses at the frequency range of operation [41], making the anti-resonant method a possible solution to the problem of frequency comb generation in the presence of nonlinear losses.

VI. CONCLUSION

We have presented an alternative, anti-resonant, approach to nonlinear optical processes at low powers, and demonstrated its application to low-power optical frequency comb generation in a silicon chip. Theoretical analysis and simulation results showed that the suggested method

operates at low intracavity and excitation powers and is not suppressed in the materials with nonlinear losses, such as silicon at the telecom wavelength.

ACKNOWLEDGEMENTS

This work was partially supported by the Air Force Office of Scientific Research under grant FA9550-12-1-0236. The authors would like to thank Prof. A. M. Weiner for helpful discussions.

- [1] A. Willner, S. Khaleghi, M. Chitgarha, and O. Yilmaz, *Journal of Lightwave Technology* **32**, 660 (2014).
- [2] R. Salem, M. A. Foster, A. C. Turner, D. F. Geraghty, M. Lipson, and A. L. Gaeta, *Nature Photonics* **2**, 35 (2008).
- [3] V. G. Ta'eed, M. Shokooh-Saremi, L. Fu, D. J. Moss, M. Rochette, I. C. M. Littler, B. J. Eggleton, Y. Ruan, and B. Luther-Davies, *Optics Letters* **30**, 2900 (2005).
- [4] M. Pelusi, V. Ta'eed, M. Lamont, S. Madden, D. Choi, B. Luther-Davies, and B. Eggleton, *IEEE Photonics Technology Letters* **19**, 1496 (2007).
- [5] S. Radic, D. J. Moss, and B. J. Eggleton, in *Optical Fiber Telecommunications V A (Fifth Edition)*, Optics and Photonics, edited by I. P. Kaminow, T. Li, and A. E. Willner (Academic Press, Burlington, 2008) pp. 759–828.
- [6] A. Alduino and M. Paniccia, *Nature Photonics* **1**, 153 (2007).
- [7] D. Miller, *IEEE Journal of Selected Topics in Quantum Electronics* **6**, 1312 (2000).
- [8] B. Lee, X. Chen, A. Biberman, X. Liu, I.-W. Hsieh, C.-Y. Chou, J. Dadap, F. Xia, W. Green, L. Sekaric, Y. Vlasov, R. Osgood, and K. Bergman, *IEEE Photonics Technology Letters* **20**, 398 (2008).
- [9] J. S. Levy, A. Gondarenko, M. A. Foster, A. C. Turner-Foster, A. L. Gaeta, and M. Lipson, *Nature Photonics* **4**, 37 (2010).
- [10] D. Woods and T. J. Naughton, *Nature Physics* **8**, 257 (2012).
- [11] H. J. Caulfield and S. Dolev, *Nature Photonics* **4**, 261 (2010).
- [12] D. Brunner, M. C. Soriano, C. R. Mirasso, and I. Fischer, *Nature Communications* **4**, 1364 (2013).
- [13] R. W. Boyd, *Nonlinear optics*, 3rd ed. (Academic Press, Burlington, MA, 2008).
- [14] T. J. Kippenberg, R. Holzwarth, and S. A. Diddams, *Science* **332**, 555 (2011).
- [15] V. Torres-Company and A. M. Weiner, *Laser & Photonics Reviews* **8**, 368 (2014).
- [16] V. Ta'eed, N. J. Baker, L. Fu, K. Finsterbusch, M. R. E. Lamont, D. J. Moss, H. C. Nguyen, B. J. Eggleton, D.-Y. Choi, S. Madden, and B. Luther-Davies, *Optics Express* **15**, 9205 (2007).
- [17] D.-I. Yeom, E. C. Mägi, M. R. E. Lamont, M. A. F. Roelens, L. Fu, and B. J. Eggleton, *Optics Letters* **33**, 660 (2008).

- [18] Q. Lin, O. J. Painter, and G. P. Agrawal, *Optics Express* **15**, 16604 (2007).
- [19] J. Aitchison, D. Hutchings, J. Kang, G. Stegeman, and A. Villeneuve, *IEEE Journal of Quantum Electronics* **33**, 341 (1997).
- [20] V. Van, T. Ibrahim, P. Absil, F. Johnson, R. Grover, and P.-T. Ho, *IEEE Journal of Selected Topics in Quantum Electronics* **8**, 705 (2002).
- [21] J. Leuthold, C. Koos, and W. Freude, *Nature Photonics* **4**, 535 (2010).
- [22] G. Steinmeyer, A. Buchholz, M. Hänsel, M. Heuer, A. Schwache, and F. Mitschke, *Physical Review A* **52**, 830 (1995).
- [23] S. Coen and M. Haelterman, *Physical Review Letters* **79**, 4139 (1997).
- [24] S. Coen and M. Haelterman, *Optics Letters* **26**, 39 (2001).
- [25] T. J. Kippenberg, S. M. Spillane, and K. J. Vahala, *Physical Review Letters* **93**, 083904 (2004).
- [26] P. Del'Haye, A. Schliesser, O. Arcizet, T. Wilken, R. Holzwarth, and T. J. Kippenberg, *Nature* **450**, 1214 (2007).
- [27] I. H. Agha, Y. Okawachi, and A. L. Gaeta, *Optics Express* **17**, 16209 (2009).
- [28] W. Liang, A. A. Savchenkov, A. B. Matsko, V. S. Ilchenko, D. Seidel, and L. Maleki, *Optics Letters* **36**, 2290 (2011).
- [29] T. Herr, K. Hartinger, J. Riemensberger, C. Y. Wang, E. Gavartin, R. Holzwarth, M. L. Gorodetsky, and T. J. Kippenberg, *Nature Photonics* **6**, 480 (2012).
- [30] S. B. Papp and S. A. Diddams, *Physical Review A* **84**, 053833 (2011).
- [31] J. Li, H. Lee, T. Chen, and K. J. Vahala, *Physical Review Letters* **109**, 233901 (2012).
- [32] L. Razzari, D. Duchesne, M. Ferrera, R. Morandotti, S. Chu, B. E. Little, and D. J. Moss, *Nature Photonics* **4**, 41 (2010).
- [33] B. J. M. Hausmann, I. Bulu, V. Venkataraman, P. Deotare, and M. Lončar, *Nature Photonics* **8**, 369 (2014).
- [34] H. Jung, C. Xiong, K. Y. Fong, X. Zhang, and H. X. Tang, *Optics Letters* **38**, 2810 (2013).
- [35] S. A. Miller, Y. Okawachi, S. Ramelow, K. Luke, A. Dutt, A. Farsi, A. L. Gaeta, and M. Lipson, *Optics Express* **23**, 21527 (2015).
- [36] F. Ferdous, H. Miao, D. E. Leaird, K. Srinivasan, J. Wang, L. Chen, L. T. Varghese, and A. M. Weiner, *Nature Photonics* **5**, 770 (2011).
- [37] Y. Liu, Y. Xuan, X. Xue, P.-H. Wang, S. Chen, A. J. Metcalf, J. Wang, D. E. Leaird, M. Qi, and A. M. Weiner, *Optica* **1**, 137 (2014).
- [38] X. Xue, Y. Xuan, Y. Liu, P.-H. Wang, S. Chen, J. Wang, D. E. Leaird, M. Qi, and A. M. Weiner, *Nature Photonics* **9**, 594 (2015).
- [39] X. Xue, Y. Xuan, P.-H. Wang, Y. Liu, D. E. Leaird, M. Qi, and A. M. Weiner, *Laser & Photonics Reviews* **9**, L23 (2015).
- [40] A. G. Griffith, R. K. W. Lau, J. Cardenas, Y. Okawachi, A. Mohanty, R. Fain, Y. H. D. Lee, M. Yu, C. T. Phare, C. B. Poitras, A. L. Gaeta, and M. Lipson, *Nature Communications* **6** (2015).

- [41] R. K. W. Lau, M. R. E. Lamont, Y. Okawachi, and A. L. Gaeta, Optics Letters **40**, 2778 (2015).
- [42] A. M. Armani, R. P. Kulkarni, S. E. Fraser, R. C. Flagan, and K. J. Vahala, Science **317**, 783 (2007).
- [43] F. Vollmer and S. Arnold, Nature Methods **5**, 591 (2008).
- [44] J. Zhu, S. K. Ozdemir, Y.-F. Xiao, L. Li, L. He, D.-R. Chen, and L. Yang, Nature Photonics **4**, 46 (2010).
- [45] V. E. Zakharov and L. A. Ostrovsky, Physica D-Nonlinear Phenomena **238**, 540 (2009).
- [46] G. Agrawal, *Nonlinear Fiber Optics* (Academic Press, 2012).
- [47] K. Ikeda, Optics Communications **30**, 257 (1979).
- [48] A. S. Rogov and E. E. Narimanov, Optics Letters **39**, 4305 (2014).
- [49] A. Coillet, I. Balakireva, R. Henriet, K. Saleh, L. Larger, J. M. Dudley, C. R. Menyuk, and Y. K. Chembo, Ieee Photonics Journal **5**, 6100409 (2013).
- [50] A. B. Matsko, A. A. Savchenkov, D. Strekalov, V. S. Ilchenko, and L. Maleki, Physical Review A **71**, 033804 (2005).